Computers & Industrial Engineering 120 (2018) 308–319

Contents lists available at ScienceDirect

Computers & Industrial Engineering

journal homepage: www.elsevier.com/locate/caie

Risk-Based X-bar chart with variable sample size and sampling interval

Zsolt Tibor Kosztyán*, Attila Imre Katona

Department of Quantitative Methods, University of Pannonia, Egyetem utca 10, Veszprém, Hungary

ARTICLE INFO

Keywords:
Adaptive control charts
Measurement uncertainty
Risk-based approach

ABSTRACT

Flexibility is increasingly important in production management, and adaptive control charts (i.e., control charts with variable sample size and/or variable sampling interval) have significant importance in the field of statistical process control. The value of the variable chart parameters depends on the detected process parameters. The process parameters need to be estimated based on observed values; however, these values are distorted by measurement uncertainty. Therefore, the performance of the method is strongly influenced by the precision of the measurement. This paper proposes a risk-based concept for the design of an *X*-bar chart with variable sample size and sampling interval. The optimal set of the parameters (control line, sample size and sampling interval) is determined using genetic algorithms and the Nelder-Mead direct search algorithm to minimize the risks arising from measurement uncertainty.

1. Introduction

For traditional control charts, a fixed sample size n, fixed sampling interval h and width coefficient of control limits k are determined. The evolution of production processes resulted in the development of more flexible control charts, where the chart parameters change based on the characteristic of the monitored process. In this case, additional levels of the chart parameters are considered. If the process is said to be "in-control", a smaller sample size, longer sampling interval and wider accepting interval are used. Conversely, in the case of an "out-of-control" process, a stricter control policy is applied (larger sample size, shorter sampling interval, and narrower accepting interval) (Lim, Khoo, Teoh, & Xie, 2015).

Reynolds, Amin, Arnold and Nachlas were the first scholars to develop an *X*-bar chart with variable sampling interval (VSI) (Reynolds, Amin, Arnold, & Nachlas, 1988), and this research inspired a number of researchers to design and improve VSI control charts (Bai & Lee, 1998; Chen, 2004; Chew, Khoo, Teh, & Castagliola, 2015; Naderkhani & Makis, 2016; Runger & Pignatiello, 1991).

Subsequently Prabhu, Runger and Keats developed an *X*-bar chart with adaptive sample size (VSS) (Prabhu, Runger, & Keats, 1993) and opened the way for research on VSS control charts (Chen, 2004; Costa, 1994; Tagaras, 1998).

As a further improvement, in VSSI control charts (variable sample size and sampling interval), the sample size and sampling interval are modified simultaneously (Chen, Hsieh, & Chang, 2007; Costa, 1997, 1998, 1999; De Magalhães, Costa, & Moura Neto, 2009). Numerous studies apply economic designs to determine the optimal parameter set for these adaptive control charts to minimize the average cost during the control process (Chen, 2004; Chen et al., 2007; Lee, Torng, & Liao, 2012; Lin, Chou, & Lai, 2009).

Adaptive control charts have had increasing interest in the recent years. Some of the more recent approaches are Safe et al. which developed VSI EWMA control chart using Multi Objective Optimization (Safe, Kazemzadeh, & Gholipour Kanani, 2018), and Yue and Liu (2017) which introduced a nonparametric EWMA chart using variable sampling interval. In another variant of the VSI control chart family, Yeong et al. designed EWMA-γ^2 chart in order to monitor the coefficient of variation (Yeong, Khoo, Tham, Teoh, & Rahim, 2017). There have been new VSS control charts developed also in the recent years (see: Aslam, Arif, & Jun, 2016; Costa & Machado, 2016; Teoh, Chong, Khoo, Castagliola, & Yeong, 2017). As final reference, we note that Salmasina et al. proposed a Hotelling's T^2 chart with variable parameters with the integration of production planning and maintenance policy as well (Salmasnia, Kaveie, & Namdar, 2018).

1.1. Control charts and risk-based aspect

Producers' and suppliers' risks are frequently discussed topics in the field of conformity or process control (see e.g.: Lira, 1999). Risks can arise from different sources, such as uncertainty in the real process parameters or imprecision of the measuring device. The effect of parameter estimation on the performance of Shewhart control charts was analyzed in several studies (see: Jensen, Jones-Farmer, Champ, &

* Corresponding author.
E-mail addresses: kzst@gtk.uni-pannon.hu (Z.T. Kosztyán), akatona@gtk.uni-pannon.hu (A.I. Katona).

https://doi.org/10.1016/j.cie.2018.04.052
Received 7 November 2017; Received in revised form 26 April 2018; Accepted 27 April 2018
Available online 01 May 2018
0360-8352/ © 2018 The Authors. Published by Elsevier Ltd. This is an open access article under the CC BY-NC-ND license (http://creativecommons.org/licenses/BY-NC-ND/4.0/).

Woodall, 2006). In addition, Zhou showed that parameter estimation has a significant effect on the in-control average time to signal (ATS) when using an adaptive VSSI X-bar chart. The study also developed an optimal design for the sample size (Zhou, 2017).

Not only uncertainty in the process parameters but also measurement uncertainty as risk factors can lead to serious consequences. If the measuring device or process is not sufficiently accurate, incorrect decisions (such as unnecessary or missed maintenance) can be made during the control of the production process (Pendrill, 2008). Thus, the rate of the producer's and customer's risk is strongly dependent on the uncertainty in the measurement and can cause loss of prestige for a manufacturer company. In many cases, the effect of measurement uncertainty is decreased by providing more accurate measuring devices or taking multiple samples Linna and Woodall (2001). Nevertheless, it is common for the improvement of a measurement device or process to run into technological limitations and it is often impossible for multiple samples to be taken due to high sampling cost (e.g., destructive sampling). To address these problems, several adjustments must be made to the control process with consideration of measurement error.

Several studied aimed to analyze the effect of measurement error on statistical control charts. Mittag and Stemann showed that gauge imprecision can strongly affect the effective application of X-S control charts and the ability to detect process shifts (Mittag & Stemann, 1998). Linna and Woodall proposed a measurement error model with covariates with the following form:

$$Y = A + BX + \epsilon \tag{1}$$

where Y is the observed value, X is the real (true) value of the monitored product characteristic, A and B are constants ($B > 1$) and ϵ is random error, which is independent of X, assuming a normal distribution with mean 0 and variance σ_m^2 ($\epsilon \sim N(0,\sigma_m^2)$) (Linna & Woodall, 2001). They investigated how measurement error (based on the referred model) influences the performance of $\overline{X}$ and S^2 charts. Several studies adopted this model and investigated the performance of different types of control charts under the presence of measurement error while assuming linearly increasing variance (Haq, Brown, Moltchanova, & Al-Omari, 2015; Hu, Castagliola, Sun, & Khoo, 2015, 2016a; Maleki, Amiri, & Ghashghaei, 2016; Maravelakis, 2012; Maravelakis, Panaretos, & Psarakis, 2004).

The impact of measurement error was considered in terms of not only the statistical but also the economical design of control charts. Rahim investigated the effect of non-normality and measurement error on the economic design of the Shewhart $\overline{X}$ chart (Rahlm, 1985). Yang extended the analysis to the asymmetric $\overline{X}$ and S charts. Yang (2002), and further studies proposed an economical design method for memory-based control charts, such as the exponentially weighted moving average (EWMA) chart based on measurement error (Abbasi, 2016; Saghaei, Fatemi Ghomi, & Jaberi, 2014). Emphasizing the importance of the effect of measurement error, several papers discussed its impact on process capability studies and proposed adjustments to improve the accuracy and reliability of the process performance indices (Baral & Anisa, 2015; Grau, 2011; Pearn, Shu, & Hsu, 2005; Wu, 2011).

Kosztyán and Katona highlighted the importance of considering the measurement uncertainty related to the multivariate T^2 chart and proposed a method to reduce the risks during the control process (Kosztyán & Katona, 2016). Their method assigns cost values to the decision outcomes and applies a risk-based approach instead of the traditional approach in statistical process control (no consideration of measurement uncertainty during the control phase). When considering measurement uncertainty, there was an˜4% decision cost reduction achieved by reducing type II errors. Although the risk-based multivariate control chart (RBT^2) reduces the cost of decision outcomes, it applies only fixed parameters (i.e., sample size, sampling interval).

This study identifies four types of decision outcomes:

- correct acceptance
- correct rejection
- incorrect acceptance (type II error)
- incorrect rejection (type I error)

The control line of a risk-based control chart is optimized to minimize the total cost arising from the four types of decision outcomes. This method achieves better performance than that when using a recommended coverage factor for the control limits.

The aim of this research is to improve the RB (risk-based) chart with variable parameters (sample size and sampling interval). The performance of the VSSI RB chart (risk-based control chart with variable sample size and sampling interval) is compared with that of the traditional control chart based on the following conditions:

1. Performance of the control chart when decision risks are not considered (k and w are chosen and n_1,h_1,n_2, and h_2 are optimized).
2. Performance of the control chart when the warning and control limits and the variable setup are optimized based on decision costs (using genetic algorithms).
3. Performance of the control chart with adjusted warning and control limits using a hybrid function to obtain more accurate results (with the Nelder-Mead direct search algorithm).

Although some studies have focused on the development of adaptive VSS (Hu, Castagliola, Sun, & Khoo, 2016b) and VSI control charts (Hu, Castagliola, Sun, & Khoo, 2016a) in the presence of measurement error, this paper aims to extend Kosztyán and Katona's model with the joint consideration of variable sample size and sampling interval (VSSI).

1.2. Traditional VSSI control charts

Consider a process with observed values following a normal distribution with expected value μ and variance σ^2. When a Shewhart control chart with fixed parameters is used, a random sample (n_0) is taken every hour (denoted by h_0). The observed statistic is plotted on the control chart, and the chart indicates when the i^{th} sample point falls outside the control limits determined as $\mu_0 \pm k\sigma\sqrt{n_0}$, where μ_0 is the center line, σ is the standard deviation of the process, and k is the control limit coefficient:

$$LCL = \mu_0 - \frac{k\sigma}{\sqrt{n_0}} \tag{2}$$

$$UCL = \mu_0 + \frac{k\sigma}{\sqrt{n_0}} \tag{3}$$

In the case of a VSSI control chart, the sample size and sampling interval vary between two levels. The first level represents a parameter set with loose control (n_1,h_1) with a smaller sample size and longer sampling interval, and the second level is a strict control policy (n_2,h_2) with a larger sample size and shorter sampling interval. The parameters n and h must satisfy the following relations: $n_1 < n_0 < n_2$ and $h_2 < h_0 < h_1$, where n_0 is the sample size and h_0 is the sampling interval of the FP control chart (control chart with fixed parameters). The switch rule between the parameter levels is based on a warning limit coefficient w. Therefore, a central region and warning region can be specified (Chen et al., 2007):

$$I_1(i) = \left[\frac{\mu_0 - w\sigma}{\sqrt{n(i)}}, \frac{\mu_0 + w\sigma}{\sqrt{n(i)}}\right] \tag{4}$$

and

$$I_2(i) = \left[\frac{\mu_0 - k\sigma}{\sqrt{n(i)}}, \frac{\mu_0 - w\sigma}{\sqrt{n(i)}}\right] \cup \left[\frac{\mu_0 + w\sigma}{\sqrt{n(i)}}, \frac{\mu_0 + k\sigma}{\sqrt{n(i)}}\right] \tag{5}$$

$$I_3(i) = \overline{I_1 \cup I_2} \tag{6}$$

where $i = 1,2...$ is the sample number, I_1 denotes the central region, and I_2 the warning region. Let us assume that an X-bar chart is applied and that $\bar{x}_i$ denotes the mean of the i^{th} sample. During the control process, the following decisions can be made (Lim et al., 2015):

1. If $\bar{x}_i \in I_1$, the manufacturing process is in an "in-control" state and sample size n_1 and sampling interval h_1 are used to compute $\bar{x}_{i+1}$.
2. If $\bar{x}_i \in I_2$, the monitored process is "in-control" but $\bar{x}_i$ falls in the warning region; thus, n_2 and h_2 are used for the $(i+1)^{th}$ sample.
3. If $\bar{x}_i \notin I_1$ and $\bar{x}_i \notin I_2$, the process is out of control, and corrective actions must be taken. After the corrective action, $\bar{x}_{i+1}$ falls into the central region, but there is no previous sample to determine $n(i+1)$ and $h(i+1)$. Therefore, as Prabhu, Montgomery, and Runger (1994) and Costa (1994) proposed, the next sample size and interval are selected randomly with probability p_0. p_0 denotes the probability that the sample mean falls within the central region. Similarly, $1-p_0$ is the probability that the sample point falls within the warning region.

VSSI control charts are a powerful tool to control manufacturing processes. However, VSSI control charts do not consider measurement uncertainty (and the risk of the decisions) as part of the control limit calculation. Due to the distortion of the measurement error, the "in-control" and "out-of-control" statements and even the switching decision between (n_1,h_1) and (n_2,h_2) can be incorrect.

2. The decision costs

Measurement uncertainty can lead to incorrect decisions during the control of a manufacturing process. Based on the model of Kosztyán and Katona (2016), the decision outcomes can be extended for a VSSI chart as follows (see Fig. 1):

Table 1 shows the possible decision outcomes when a VSSI control chart is applied. Due to the distortion effect of the measurement uncertainty, the real product characteristic can differ from the observed product characteristic, resulting in incorrect decisions. In Table 1, "in (CL)" and "out(CL)" denote the in-control and out-of-control statements based on the control line(s), and "in(WL)" and "out(WL)" represent the sample location relative to the warning limits. In addition, $x$is the real product characteristic, and y is the detected one. I_1, I_2 and I_3 denote the regions according to Eqs. (2)–(4). If the detected characteristic falls within the out-of-control region based on the control line, it excludes the potential of being "in-control" based on the warning limit.

Table 1
Elements of the cost of decision outcomes.

Sign	Name
n	Sample size
N_h	Produced quantity in the considered interval (h)
c_p	Production cost
c_{mf}	Fixed cost of measuring
c_{mp}	Proportional cost of measuring
c_c	Cost of qualification
c_s	Cost of switching
d_1	Weight parameter for switching
c_i	Cost of intervention
d_2	Weight parameter for intervention
c_r	Cost of root cause search
c_{id}	Cost of delayed detection
c_f	Cost of false alarm identification
c_{mi}	Cost of missed intervention
c_r	Cost of restart
c_{ma}	Maintenance cost

Similarly, if the real product characteristic is out-of-control (based on the control lines), the sample point cannot fall within the central region. These cases are represented by a black cross in the table. Each case can be described as follows (the number of each case is represented by number in the right left corner of each cell in the table):

- Case 1: Both the detected and the real product characteristic fall within the central region. The decision is a correct acceptance.
- Case 2: The detected characteristic is in the warning region but the real characteristic is in the central region. In this case, the sample size is increased and the sampling interval is reduced. However, these changes are unnecessary, and the decision is incorrect.
- Case 3: The process is out-of-control based on the detected product characteristic, but the real characteristic falls within the central region. The expected value of the process is in-control, but a shift is detected incorrectly. Therefore, an unnecessary corrective action is taken (type I error).
- Case 4: The real characteristic is within warning region (out-of-control based on the warning limit) but an in-control statement is detected. In this case, the sample size should be increased and the sampling interval should be reduced; however, this action is not taken. This failure reduces the performance of the VSSI chart because it increases the time for detection and correction.

			Detected product characteristic			
			in (CL)		out (CL)	
			in (WL)	out (WL)	in (WL)	out (WL)
Real	in (CL)	in (WL)	$x \in I_1$ and $y \in I_1$ (1)	$x \in I_1$ and $y \in I_2$ (2)		$x \in I_1$ and $y \in I_3$ (3)
		out (WL)	$x \in I_2$ and $y \in I_1$ (4)	$x \in I_2$ and $y \in I_2$ (5)		$x \in I_2$ and $y \in I_3$ (6)
	out (CL)	in (WL)				
		out (WL)	$x \in I_3$ and $y \in I_1$ (7)	$x \in I_3$ and $y \in I_2$ (8)		$x \in I_3$ and $y \in I_3$ (9)

Fig. 1. The structure of decision outcomes.

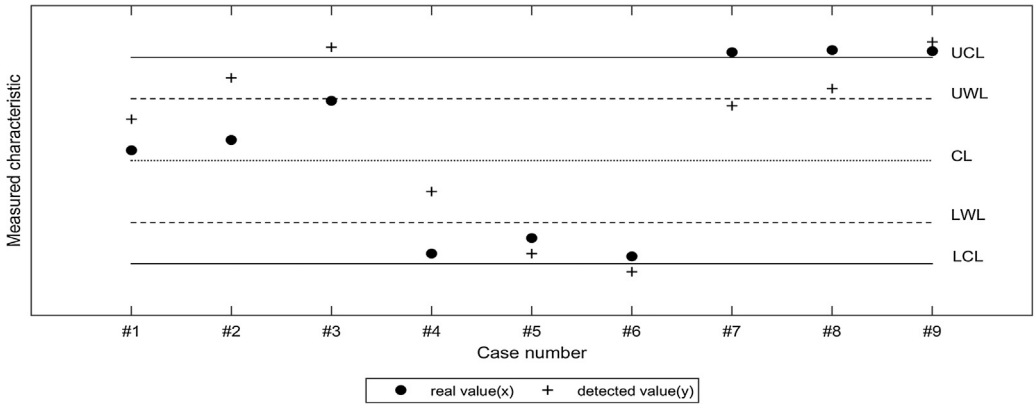

Fig. 2. Demonstration of the nine decision outcomes on a control chart.

- Case 5: Both the detected and real characteristics fall within the warning region. The sample size is increased, the sampling interval is reduced, and the decision is correct.
- Case 6: Out-of-control is detected; however, the real characteristic falls within the warning region. Corrective action is taken, but the switch between the chart parameters (n,h) would be sufficient. Therefore, the decision is incorrect.
- Case 7: In-control state is detected and y is located in the central region, but the process is out-of-control. The decision is incorrect, and corrective action is not taken, which is a type II error.
- Case 8: Similar to Case 7, but y is in the warning region. Therefore, this case is more positive than Case 7 because a strict control policy is applied. Thus, a shorter time is needed to identify the process shift.
- Case 9: The real and detected product characteristics are out-of-control; therefore, the decision is correct.

For clarification, Fig. 2 shows an example of the nine decision outcomes described above.

2.1. Specification of decision costs

During process control, several decisions can be made. In this subsection, we introduce the cost structure of each decision outcome. First, the elements of the decision outcomes must be specified.

Table 1 shows the specified cost components in the cost structure. The following costs are involved in each decision:

- expected total production cost
- cost of measuring
- cost of qualification

c_p denotes the proportional production cost, and N_h is the expected number of manufactured products in interval h (where h is the time interval between two samples). Therefore, the expected total production cost can be estimated as $N_h c_p$. The cost of measurement can be divided into two parts, a fixed cost (c_{mf}) and a proportional cost (c_{mp}) depending on sample size (n). The fixed measurement cost (e.g., labor, lighting, operational cost of the measurement device) arises in every measurement irrespective of n. c_{mp} is the expected measurement cost for a sample that strongly depends on sample size (especially significant for destructive measurement processes). Thus, the expected total measurement cost can be estimated as $nc_{mp} + c_{mf}$. In addition, the cost of qualification c_q must be considered (charting, plotting, labor). Since $N_h c_p + nc_{mp} + c_{mf} + c_q$ is a part of each cost component, we apply a constant $N_h c_p + nc_{mp} + c_{mf} + c_q = c_0$ for simplicity.

Some cost components arise in only special cases. The cost of switching c_s is the cost of the modification of the VSSI chart parameters (n,h). c_i denotes the cost of intervention, including the cost of the machine stop and root cause search. If the root cause cannot be identified, it is likely that a false alarm occurred. In this case, the cost of maintenance (c_{ma}) cannot be specified. On the other hand, this cost component must be considered when a root cause is found and the machine must be maintained (e.g., cost of the parts, labor cost).

The weighting parameters must also be specified. Some cases (e.g., Case 2 and Case 5) are similar but have different estimated costs. This difference can be derived from the necessity of the decision. For example, in Cases 2 and 5, the detected characteristic is located in the warning region but the decision is necessary in Case 2 and unnecessary in Case 5. In similar cases, the unnecessary decision must be multiplied by the weighting parameter to consider the surplus modifications during control. Therefore, d_1 is the weighting parameter for the cost of unnecessary switching, and d_2 is the weighting parameter for unnecessary intervention. Table 2 includes the forms of the decision costs assigned to the decision outcomes.

During the control process, sufficient cost must be assigned to each sampling point. The assigned costs must be further aggregated to determine the total decision cost from the first sample to the actual one. The goal is to set the optimal value of the coverage factor k (and the optimal values of the control lines UCL,LCL) and the optimal parameter set for the switching (n,h) to minimize the total decision cost. A detailed introduction for this optimization method is provided in Section 3.

3. The RB VSSI *X*-bar chart

3.1. Overview of the proposed chart construction method

In this subsection, the authors introduce the construction process of the RB VSSI X-bar chart, which can be summarized as follows:

1. Calculation of the traditional control chart parameters (as initial values for the optimization).

Table 2
Elements of the costs of the decision outcomes.

Case	Structure	Simplified form
#1	$C_1 = N_h c_p + nc_{mp} + c_{mf} + c_q$	$C_1 = c_0$
#2	$C_2 = N_h c_p + nc_{mp} + c_{mf} + c_q + d_1 c_s$	$C_2 = c_0 + d_1 c_s$
#3	$C_3 = N_h c_p + nc_{mp} + c_{mf} + c_q + d_2 c_i$	$C_3 = c_0 + d_2 c_i$
#4	$C_4 = N_h c_p + nc_{mp} + c_{mf} + c_q + c_{id}$	$C_4 = c_0 + c_{id}$
#5	$C_5 = N_h c_p + nc_{mp} + c_{mf} + c_q + c_s$	$C_5 = c_0 + c_s$
#6	$C_6 = N_h c_p + nc_{mp} + c_{mf} + c_q + d_2 c_i$	$C_6 = c_0 + d_2 c_i$
#7	$C_7 = N_h c_p + nc_{mp} + c_{mf} + c_q + c_{mi}$	$C_7 = c_0 + c_{mi}$
#8	$C_8 = N_h c_p + nc_{mp} + c_{mf} + c_q + d_3 c_{mi}$	$C_8 = c_0 + c_{mi}$
#9	$C_9 = N_h c_p + nc_{mp} + c_{mf} + c_q + c_{ma} + c_r$	$C_9 = c_0 + c_r$

2. Estimation of the cost components described in Section 2.
3. Calculation of the overall decision cost considering the initial (traditional) control chart parameters.
4. Optimization of the control chart parameters via simulation.
   (a) Control chart parameter optimization via genetic algorithm.
   (b) Improvement of the optimization result using the Nelder-Mead direct search method.

In the following, we describe the above steps in detail.

Step 1:

The control lines of the traditional X-bar chart can be computed with (2) and (3). The VSSI RB X-bar chart uses these control lines as initial values. During optimization, the optimal values of UCL and LCL that minimize the total decision cost are determined by simulation.

Step 2:

The cost values for each case ($C1$,$C2$,...$C9$) must be estimated. This can be supported by an ERP system, where the estimated costs can be queried from a control module. Otherwise, each cost component should be estimated by experts. Each cost must be assigned to the suitable case (according to Table 1) to calculate the total decision cost during the simulation (or during the control process).

Step 3:

The number of occurrences each case must be quantified and multiplied by the assigned cost value. In the cost structure, $N_h c_p + nc_{mp} + c_{mf} + c_q$ is the cost component that arises in every case; therefore, to simplify the formula, it is replaced with C_c.

$$\begin{aligned}\sum C = {} & q_1 C_c + q_2(C_c + d_1 c_s) + q_3(C_c + d_2 c_i) + q_4(C_c + c_{id}) + q_5(C_c + c_s) \\ & + q_6(C_c + d_2 c_i) + q_7(C_c + c_{mi}) + q_8(C_c + d_3 c_{mi}) \\ & + q_9(C_c + c_{ma} + c_r)\end{aligned} \tag{7}$$

where q_1,q_2...q_9 are the numbers of time each case occurs during the simulation and $\sum C$ is the total decision cost. The equation can be simplified using the cost values of each decision outcome:

$$\sum C = q_1 C_1 + q_2 C_2 + q_3 C_3 + q_4 C_4 + q_5 C_5 + q_6 C_6 + q_7 C_7 + q_8 C_8 + q_9 C_9 \tag{8}$$

Step 4:

The coverage factor k and the variable parameters (n_1,n_2,h_1,h_2,w) are optimized to minimize the value of $\sum C$. Two approaches are used to optimize the chart parameters. The integer parameters, (n_1,n_2,h_1,h_2) are optimized using genetic algorithms as the first step. In the second step, the Nelder-Mead algorithm is used as a hybrid function. This approach optimizes the continuous parameters (k,w) to obtain more precise results for the modified warning and control limits.

3.2. Simulation of the control procedure and optimization

As the first step, an $n \times m$ matrix (denoted by $\mathbf{X}$) of the "real" values is generated with expected value μ_x and standard deviation σ_x. Similarly, an $n \times m$ matrix $\mathbf{E}$, representing the measurement error, is also generated. We use Matlab's "pearsrnd" function to generate the measurement error matrix. This function returns an $n \times m$ matrix of random numbers according to the distribution in a Pearson system. With this approach, the four parameters (expected value, standard deviation, skewness and kurtosis) of the measurement error distribution can be easily modified.

After these two matrices are generated, the matrix of "observed" values can be estimated in the following manner:

$$\mathbf{Y} = A + B\mathbf{X} + \mathbf{E} \tag{9}$$

where $\mathbf{Y}$ is an $n \times m$ matrix containing the estimated observed values.

In both $\mathbf{X}$ and $\mathbf{Y}$, each row represents a possible sampling event and each element in a row represents all the possible products that can be selected for sampling. To construct the VSSI X-bar chart, the VSSI rules must be applied to $\mathbf{X}$ and $\mathbf{Y}$. The algorithm loops through the matrices from the first row to the n^{th} row.

Let $\hat{x}$ be the vector of sample means from $\mathbf{X}$, and let $\hat{y}$ be the vector of sample means selected from $\mathbf{Y}$. If the i^{th} sample mean (with sample size n_1) falls within the warning region, n_2 and h_2 must be used in the next sampling:

a. If $\hat{x}_j \in I_2$, then the $i + h_2^{th}$ row from $\mathbf{X}$ is selected for sampling and element n_2 is selected randomly from the $i + h_2^{th}$ row. Otherwise, the $i + h_1^{th}$ row is selected with sample size n_1.
b. If $\hat{y}_j \in I_2$, then the $i + h_2^{th}$ row from $\mathbf{Y}$ is selected for sampling and element n_2 is selected randomly from the $i + h_2^{th}$ row. Otherwise, the $i + h_1^{th}$ row is selected with sample size n_1.

In the next step, each element in $\hat{x}$ and $\hat{y}$ is compared and assigned to a decision outcome described in Section 2. In the final step of the simulation, the total decision cost is calculated as the summation of the cost of each decision.

We use genetic algorithms to find the optimal set of integer design parameters (n_1,n_2,h_1,h_2) that minimizes the total cost function given by Eq. (8). This approach imitates the principles of natural selection and can be applied to estimate the optimal design parameters for statistical control charts. In the first step, this method generates an initial set of feasible solutions and evaluates them based on a fitness function. In the next step, the algorithm:

(1) selects parents from the population;
(2) creates crossover from the parents;
(3) performs mutation on the population given by the crossover; operator
(4) evaluates the fitness value of the population.

This steps are repeated until the algorithm finds the best fitting solution (Chen et al., 2007). Then, the Nelder-Mead method is applied as a hybrid function to search for the optimal values of the continuous variables (w,k).

This is a two-dimensional case, where the algorithm generates a sequence of triangles converging to the optimal solution. The objective function is $C(n_1,n_2,h_1,h_2,w,k)$, where w is the warning limit coefficient and k is the control limit coefficient. Note that the other design parameters (n_1,n_2,h_1,h_2) are already optimized by genetic algorithms; therefore, in this step, we use the objective function $C(w,k)$, where $0 < w < k$ and $w,k \in \mathbb{R}$.

In the two-dimensional case, three vertices must be determined, and the cost function is evaluated for each vertex. In the first step, ordering is performed on the vertices:

Ordering:

The vertices must be ordered based on the evaluated values of the cost function:

$$C_B(w_1,k_1) < C_G(w_2,k_2) < C_W(w_3,k_3) \tag{10}$$

where C_B is the best vertex with the lowest total cost, C_G (good) is the second-best solution and C_W is the worst solution (with the highest cost value). Furthermore, let $\boldsymbol{v}_1 = (w_1,k_1)$,$\boldsymbol{v}_2 = (w_2,k_2)$ and $\boldsymbol{v}_3 = (w_3,k_3)$ denote the vectors of each point.

The approach applies four operations: reflection, expansion, contraction and shrinking.

Reflection:

The reflection point is calculated as:

$$\begin{aligned}\mathbf{v}_R &= [w_R,k_R]^T \\ &= \left[\frac{w_1 + w_2}{2} + \alpha\left(\frac{w_1 + w_2}{2} - w_3\right), \frac{k_1 + k_2}{2} + \alpha\left(\frac{k_1 + k_2}{2} - k_3\right)\right]^T \\ &= \frac{\mathbf{v}_1 + \mathbf{v}_2}{2} + \alpha\left(\frac{\mathbf{v}_1 + \mathbf{v}_2}{2} - \mathbf{v}_3\right)\end{aligned} \tag{11}$$

where $\mathbf{v}_R$ is a vector denoting the reflection point, w_R,k_R are the

coordinates of the reflection point and $\alpha > 1$ is the reflection parameter. $C_R(w_R,k_R)$ must be evaluated, and $\mathbf{v}_3$ needs to be replaced with $\mathbf{v}_R$ if $C_B(w_1,k_1) \leqslant C_R(w_R,k_R) < C_G(w_2,k_2)$.

Expansion:

After reflection, expansion is performed if $C_R(w_R,k_R) < C_B(w_B,k_B)$:

$$\begin{aligned}\mathbf{v}_E &= [w_E,k_E]^T \\ &= \left[\frac{w_1+w_2}{2} + \beta\left(w_R - \frac{w_1+w_2}{2}\right), \frac{k_1+k_2}{2} + \beta\left(k_R - \frac{k_1+k_2}{2}\right)\right]^T \\ &= \frac{\mathbf{v}_1+\mathbf{v}_2}{2} + \beta\left(\mathbf{v}_R - \frac{\mathbf{v}_1+\mathbf{v}_2}{2}\right)\end{aligned} \tag{12}$$

where $\mathbf{v}_E$ denotes the reflection point with coordinates w_E and k_E and β is the expansion parameter. $C_E(w_E,k_E)$ is evaluated and $\mathbf{v}_3$ is replaced with $\mathbf{v}_E$ if $C_E(w_E,k_E) \leqslant C_R(w_R,k_R)$.

Contraction:

Outside contraction is performed if $C_G(w_2,k_2) \leqslant C_R(w_R,k_R) < C_W(w_3,k_3)$:

$$\begin{aligned}\mathbf{v}_{OC} &= [w_{OC},k_{OC}]^T \\ &= \left[\frac{w_1+w_2}{2} + \gamma\left(w_R - \frac{w_1+w_2}{2}\right), \frac{k_1+k_2}{2} + \gamma\left(k_R - \frac{k_1+k_2}{2}\right)\right]^T \\ &= \frac{\mathbf{v}_1+\mathbf{v}_2}{2} + \gamma\left(\mathbf{v}_R - \frac{\mathbf{v}_1+\mathbf{v}_2}{2}\right)\end{aligned} \tag{13}$$

Here, $\mathbf{v}_{OC}$ is the point that can be derived by outside contraction with coordinates w_{OC} and k_{OC}; furthermore, $0 < \gamma < 1$ is the contraction parameter. Then, evaluate $C_{OC}(w_{OC},k_{OC})$. If $C_{OC}(w_{OC},k_{OC}) \leqslant C_R(w_R,k_R)$, replace $\mathbf{v}_3$ with $\mathbf{v}_{OC}$; otherwise, the shrinking operation must be performed.

The inside contraction point denoted by $\mathbf{v}_{IC}$ is computed if $C_R(w_R,k_R) \geqslant C_W(w_3,k_3)$:

$$\begin{aligned}\mathbf{v}_{IC} &= [w_{IC},k_{IC}]^T \\ &= \left[\frac{w_1+w_2}{2} - \gamma\left(w_R - \frac{w_1+w_2}{2}\right), \frac{k_1+k_2}{2} - \gamma\left(k_R - \frac{k_1+k_2}{2}\right)\right]^T \\ &= \frac{\mathbf{v}_1+\mathbf{v}_2}{2} - \gamma\left(\mathbf{v}_R - \frac{\mathbf{v}_1+\mathbf{v}_2}{2}\right)\end{aligned} \tag{14}$$

In this case, $C_{IC}(w_{IC},k_{IC})$ is evaluated, and the point with the highest total decision cost $\mathbf{v}_3$ is replaced with $\mathbf{v}_{IC}$; otherwise, the shrinking operation is used.

Shrinking:

Shrinking must be performed for the n^{th} and $n+1^{th}$ points. Since we consider the two-dimensional case of the design parameters w and k, this operation is performed for $\mathbf{v}_2$ and $\mathbf{v}_3$:

$$\mathbf{v}_{2S} = [w_{2S},k_{2S}]^T = [w_1 + \delta(w_2 - w_1), k_1 + \delta(k_2 - k_1)]^T = \mathbf{v}_1 + \delta(\mathbf{v}_2 - \mathbf{v}_1) \tag{15}$$

$$\mathbf{v}_{3S} = [w_{3S},k_{3S}]^T = [w_1 + \delta(w_3 - w_1), k_1 + \delta(k_3 - k_1)]^T = \mathbf{v}_1 + \delta(\mathbf{v}_3 - \mathbf{v}_1) \tag{16}$$

where $\mathbf{v}_{2S}$ and $\mathbf{v}_{3S}$ are the shrunk points derived from $\mathbf{v}_2$ and $\mathbf{v}_3$, respectively (Fan, Liang, & Zahara, 2006).

4. Practical example

In this section, we demonstrate the applicability of the proposed method with a practical example. Table 3 shows the cost of the nine decision outcomes as input parameters.

Furthermore, the production process follows a normal distribution with expected value $\mu_x = 100$ and standard deviation $\sigma_x = 0.2$. The measurement error has a normal distribution with expected value $\mu_m = 0$ and standard deviation $\sigma_m = 0.02$. In the first step, $k = 3$ and $w = 2$ are used to calculate the control and warning limits (k is the control limit coefficient an w is the warning limit coefficient). The other design parameters (n_1,n_2,h_1,h_2) are optimized to minimize the total cost of the decisions, as described by Eq. (8). Next, the design parameters k and w are optimized using the Nelder-Mead direct search method. In this study, k^* and w^* denote the optimal values of k an w. Fig. 3 shows the value of the objective function in each iteration of the optimization.

Table 3
Elements of the cost of the decision outcomes.

Case	Structure	Value
#1	$C_1 = N_h c_p + n c_{mp} + c_{mf} + c_q$	1
#2	$C_2 = N_h c_p + n c_{mp} + c_{mf} + c_q + d_1 c_s$	5
#3	$C_3 = N_h c_p + n c_{mp} + c_{mf} + c_q + d_2 c_i$	50
#4	$C_4 = N_h c_p + n c_{mp} + c_{mf} + c_q + c_{id}$	7
#5	$C_5 = N_h c_p + n c_{mp} + c_{mf} + c_q + c_s$	3
#6	$C_6 = N_h c_p + n c_{mp} + c_{mf} + c_q + d_2 c_i$	50
#7	$C_7 = N_h c_p + n c_{mp} + c_{mf} + c_q + c_{mi}$	600
#8	$C_8 = N_h c_p + n c_{mp} + c_{mf} + c_q + d_3 c_{mi}$	550
#9	$C_9 = N_h c_p + n c_{mp} + c_{mf} + c_q + c_{ma} + c_r$	20

In Fig. 3, the circles represent the actual values of the objective function when the genetic algorithm is running. Similarly, the triangles show the objective function values during the Nelder-Mead approach. The Nelder-Mead method achieves an additional 0.5% cost reduction, but more importantly, the results derived from the hybrid function are more stable.

Table 4 shows the results of the proposed method.

The total cost of decisions is reduced by 13.5% when applying the proposed method. The integer parameters (n_1,n_2,h_1,h_2) are optimized in the initial state to minimize the total cost of decisions.

Kosztyán et al. proposed a risk-based approach for conformity control (Kosztyán, Hegedűs, & Katona, 2017), and another study developed a risk-based multivariate T^2 chart (Kosztyán & Katona, 2016). Both approaches achieved an approximately 2–4% reduction in the total decision cost. However, as the previous example shows, the VSSI X-bar chart outperforms the traditional X-bar chart, and the proposed method reduced the total decision cost by 13.5%. To explain the outstanding reduction rate, in Fig. 4, we highlight an interval from the time series of the controlled product characteristic to compare the behavior and patterns of the risk-based and traditional VSSI X-bar charts.

The traditional control chart is shown in the upper-left corner of Fig. 4, where the control and warning lines were set to their initial values (measurement uncertainty was not considered), $\overline{X}$ denotes the sample mean of the real (simulated) product characteristic, and $\overline{Y}$ denotes the sample mean of the observed product characteristic (simulated measurement error is added to X). The bar chart in the lower-left corner shows the cost value assigned to each decision (to each plot of the time series). Similarly, the right side of the chart shows the pattern if the risk-based VSSI X-bar chart is used and the control and warning limits are optimized while taking the measurement uncertainty into account.

In the case of the adaptive control chart, the pattern of the control chart depends not only on the values of the control limits but also on the width of the warning interval. The sample size and sampling interval are determined by the position of the observed sample mean and warning limits. Therefore, the distorting effect of the measurement error can create very different scenarios based on the control chart patterns. If the observed sample mean falls within the warning region and the real sample mean is located within the acceptance interval, the sample number will be increased and the sampling interval will be reduced incorrectly, leading to increased sampling costs. In the opposite case, sampling will be skipped, which will delay the detection of the process mean shift.

As shown in Fig. 4, when the traditional VSSI chart is applied, the two process patterns (observed and real) become separated from each other by the 7^{th} sampling. A different sampling policy will then be used due to the effect of the measurement uncertainty, causing separation of

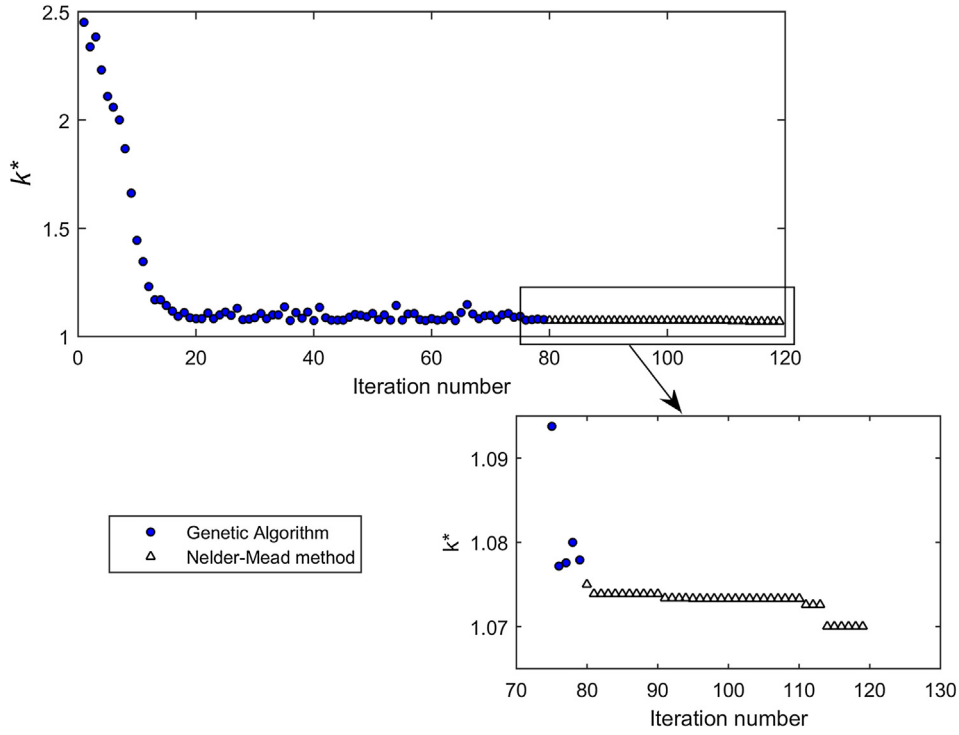

Fig. 3. Convergence to the optimal solution with Genetic Algorithm and Nelder-Mead direct search.

Table 4
Performance of the proposed control chart.

	n_1	n_2	h_1	h_2	k^*	w^*	$\sum C$	$\Delta C(\%)$
Initial state	2	4	2	1	3.00	2.00	1.236E + 06	–
Optimization: GA	2	4	2	1	2.298	2.287	1.075E + 06	−13.0
Optimization: GA + NM	2	4	2	1	2.298	2.175	1.070E + 06	−13.5

the two control chart patterns. The sifted pattern continues until the point, where the two control policy is the same again. On the other hand, the risk-based VSSI *X*-bar chart takes measurement uncertainty into account and modifies the warning interval, enabling better fitting of the two control chart patterns. The shifted interval is denoted by the dark columns on the bar charts. The charts show that the RB VSSI chart reduces the length of the interval. Therefore, it reduces not only the decision costs due to the out-of control state but also decreases the number of incorrect decisions in the in-control state and compensates for the separation of the chart patterns. Therefore, a greater decision-cost reduction can be achieved with the VSSI chart compared to the

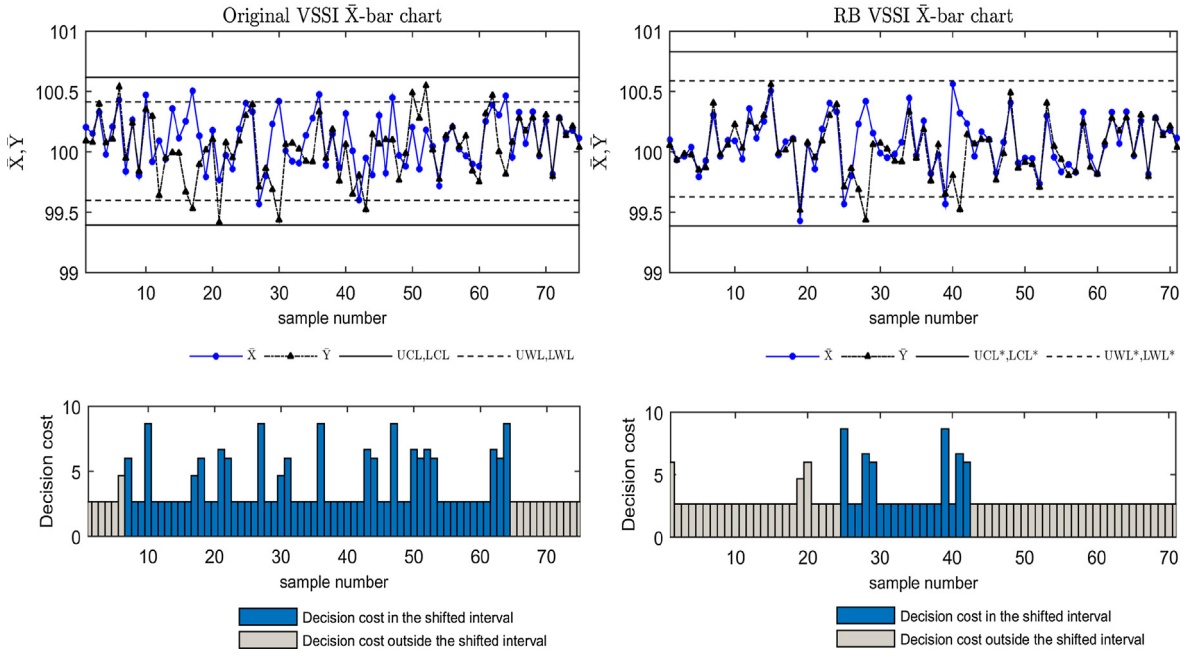

Fig. 4. Comparison traditional and RB VSSI control chart patterns.

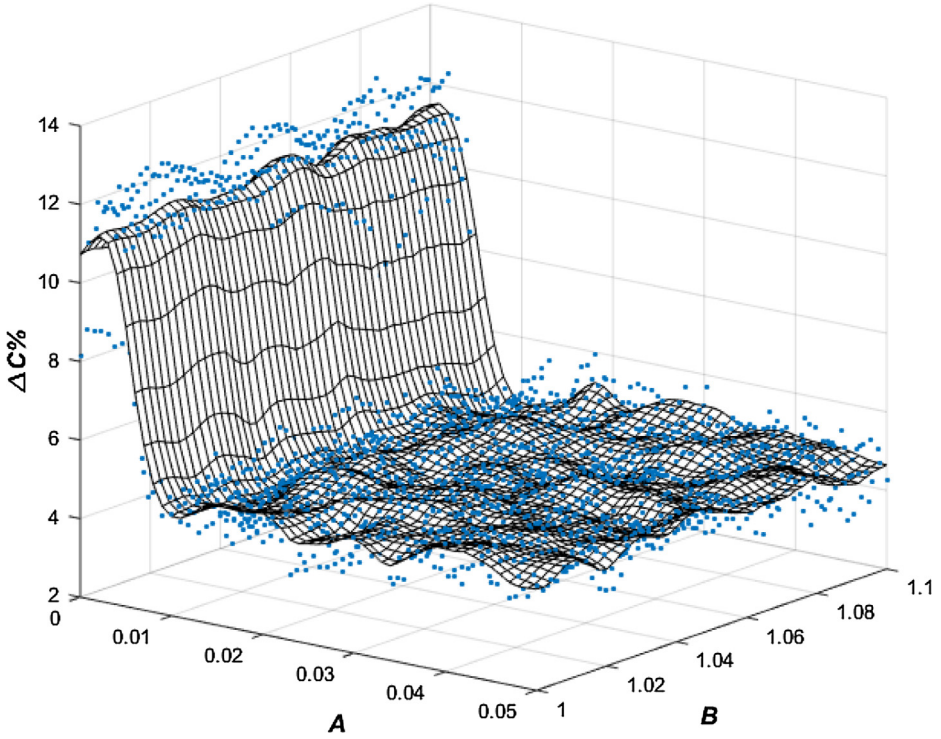

Fig. 5. The cost reduction rate as a function of A and B.

results of the referenced studies.

As a significant contribution, this paper also raises awareness of the importance of considering measurement uncertainty in the field of adaptive control charts.

In the practical example, the authors applied the $Y = A + BX + \varepsilon$ model of measurement error under the assumption of constant variance ($A = 0$ *and* $B = 1$). To investigate how the proposed model performs under linearly increasing variance, an additional simulation was conducted. Fig. 5 shows the results of the simulation.

We used the same cost components as described in Table 3, but parameters A and B in the measurement error equation were changed in each iteration. The z-axis shows the achievable cost reduction rate expressed as a percentage ($\Delta C\%$) for each combination of A and B. The blue dots show the raw results of the simulation, and a smoothed pane was fitted to the data points to better illustrate the pattern. The results show that the proposed method still reduces the overall decision cost under linearly increasing measurement error variance; however, the model is sensitive to changes in parameter A (changes in parameter B do not significantly alter the cost reduction). If $A > 0$, the distance between X and Y increases significantly, indicating shorter sampling intervals and larger sample sizes. Although the proposed method achieves lower overall decision cost through modification of the warning and control limits, the increased cost from sampling increases the overall decision cost, limiting the cost reduction for the method. Nevertheless, an approximately 4% cost reduction was achieved under linearly increasing variance due to the optimization of the control and warning limits.

5. Sensitivity analysis

Section 4 demonstrated the applicability of the method for the given example. The purpose of this section is to investigate the more general behavior (pattern) of the control chart parameters. Therefore, we analyze how changes in the cost components, standard deviation of the measurement error and skewness of the measurement error impact the value of k^* and w^*. These factors are selected to assess the limitations of the proposed method. The kurtosis of the measurement error could also be examined, but its impact was previously analyzed by Kosztyán et al. The cost of type II errors is analyzed first.

5.1. Sensitivity analysis with respect to the cost of type II error

The 9 decision outcomes defined in this study must be assigned to different groups for a better understanding of the effects during the sensitivity analysis.

Therefore, we distinguish three groups of decision outcomes:

- Group 1: Type I error decision outcomes, where the decision is incorrect due to an unnecessary action. Outcomes: #2, #3, #6.
- Group 2: Type II error decision outcomes, where the decision is incorrect due to a missed action. Outcomes: #4, #7, #8.
- Group X: The remaining decision outcomes, including the correct decisions. Outcomes: #1, #5, #9.

During the sensitivity analysis, each cost in Group 2 is multiplied by a changing coefficient (a). Thus, the i^{th} cost is calculated as:

$$C_{4_i} = a_i \cdot C_{4_{initial}} \tag{17}$$

$$C_{7_i} = a_i \cdot C_{7_{initial}} \tag{18}$$

$$C_{8_i} = a_i \cdot C_{8_{initial}} \tag{19}$$

where $C_{4_{initial}}, C_{7_{initial}}$, *and* $C_{8_{initial}}$ are the initial values of the decision costs related to cases #4, #7, and #8. a_i is the value of the coefficient in the i^{th} run within the simulation, and $i = 1,2,3...n, i \in \mathbb{N}$ where n is the total number of runs. Fig. 6 shows the optimal values of k and w (denoted by k^* and w^*) as a function of the cost-changing coefficient a.

In Fig. 6, the circles represent the values of k^* and the crosses indicate the values of w^*. While C_4,C_7 and C_8 increase, the optimal values of both k and w decrease. If the cost of type II error decisions increases, the control policy will be stricter. Therefore, the control and warning limits must be moved closer to the central line of the control chart to avoid type II errors. An increase in type II-related costs does not have a significant impact on the interval between k^* and w^*. As a increases, the

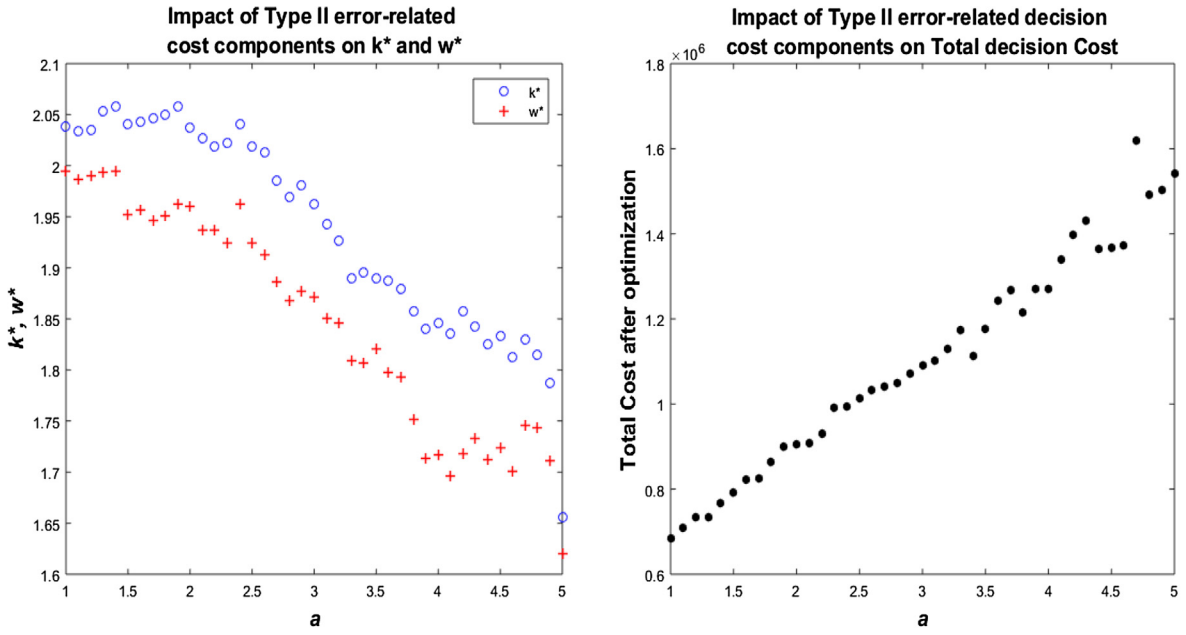

Fig. 6. Sensitivity analysis regarding type II error-related cost components.

control and warning limits move in the same direction simultaneously. The impact of the type II error-related cost components on the overall decision cost was also investigated. As the results on the right side of Fig. 6 show, the overall decision cost increases linearly with parameter a. Note that the analysis shows the overall decision cost after optimization. Although this method reduces the risk, the overall decision cost is higher if the consequences of type II errors are more serious.

To further analyze the behavior of the warning interval, we conducted a sensitivity analysis based on the sampling cost because it directly influences the warning limit coefficient. Fig. 7 shows the results of the analysis.

Fig. 7 shows the distance between k^* and w^* (k^*-w^*) as a function of the sampling cost (c_s). The higher the cost of sampling is, the greater the distance between the two limits. A higher sampling cost increases the warning limit coefficient because the control is too expensive due to the frequently increased sample size and sampling interval. A lower sampling cost allows a stricter control policy for the warning limit.

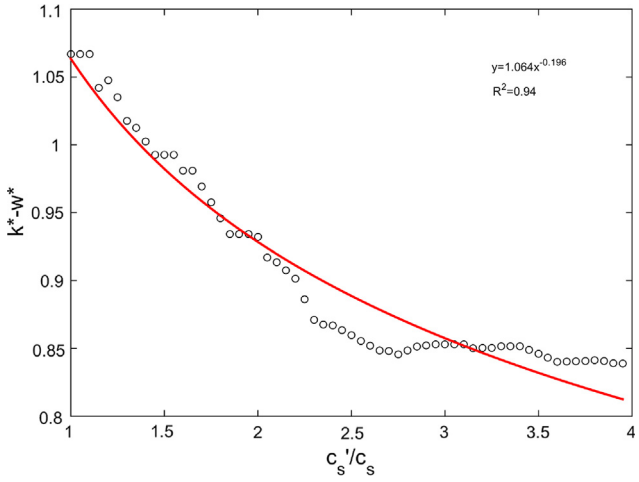

Fig. 7. The width of warning interval as a function of sampling cost.

5.2. Sensitivity analysis based on the standard deviation of the measurement error

The behavior of the control limits was also examined while changing the standard deviation in the simulation. All the distribution parameters were held constant during the simulation except the standard deviation of the measurement error (σ_m).

As Fig. 8 shows, the control limit coefficients (w^* and k^*) decrease as the standard deviation of the measurement error increases. A higher standard deviation (according to the measurement error) represents a stricter control policy; thus, w^* and k^* decrease. In this case, the effect of measurement uncertainty is increasingly significant; therefore, the approach reduces the length of the control interval to avoid type II errors. The distance between the two limits is nearly constant because the sampling cost does not change during the simulation. Nevertheless, the sampling cost has a significant impact on the distance between w^* an k^*, as shown in the previous subsection. The results show that σ_m significantly affects the overall decision cost. A higher standard deviation of the measurement error results in a higher frequency of control measures, causing higher costs.

5.3. Sensitivity analysis base on the skewness of the measurement error

Since Kosztyán et al. proved that the kurtosis of the measurement error distribution does not impact the control line value, we focus on the skewness of the measurement error distribution only.

In the simulation, the model parameters were the same, but the skewness of the measurement error distribution (denoted by γ) was modified in each iteration (starting with -1 and ending with 1).

Fig. 9 shows the results of the sensitivity analysis.

In the simulation, k^* and w^* are not affected by changes in γ because sampling adjusts the skewed distribution to normal. Based on the central limit theorem, the average of the aggregated sample groups tend to normal (and the skewness will be more closer to 0). An illustrative example from the simulation is shown in the appendix in Fig. 10.

This phenomenon is also reflected by the results related to the overall decision cost. Due to the central limit theorem, neither the limit coefficients k^* and w^* nor the overall decision cost react to changes in the skewness of the measurement error distribution.

In this section, the model sensitivity was analyzed from different

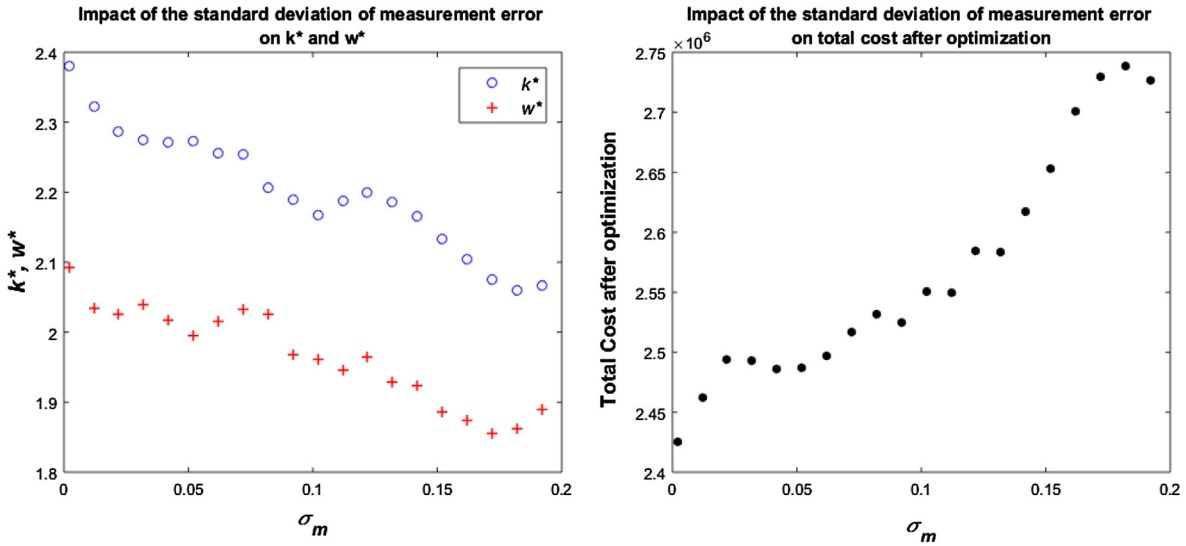

Fig. 8. Sensitivity analysis regarding standard deviation of measurement error.

aspects; however, we note that uncertainty related to the process parameter estimation can also affect the control chart parameters (Zhou, 2017). This paper focuses on the effect of measurement uncertainty and proposes a method to develop a risk-based adaptive control charts. Nevertheless, the method can be extended to consider the process parameter estimation.

6. Summary and conclusion

This paper extends the consideration of measurement uncertainty to the field of adaptive control charts. The proposed method not only optimizes the chart parameters (n_1,n_2,h_1,h_2,k,w) but also adjusts the control and warning limit coefficients (k^*, and w^*) to minimize the aggregated cost derived from the decision outcomes. Genetic algorithm and the Nelder-Mead method (as a hybrid function) are used during the chart-parameter optimization. A practical example is provided to demonstrate the features of the proposed method. With the assumed inputs, the proposed method reduces the total decision cost by 13.5% compared to the "traditional" VSSI X-bar chart (due to the reduction of incorrect decisions). Several sensitivity analyses are also provided to assess the behavior of the optimized parameters k^*,w^* and the overall decision cost (providing more general conclusions compared to those from the practical example).

The contribution of the proposed method can be defined from two aspects. As an academic contribution, this study extends the dimension of the decision matrix defining decision outcomes regarding the warning limits as well. In addition the results showed that measurement uncertainty can be described by the first two moments of its distribution function (expected value and standard deviation) when the RB VSSI chart is applied because the result of the optimization is not sensitive to the skewness of the distribution. From decision maker's point of view, the results show that consideration of measurement uncertainty is important not only from control lines' perspective but decision costs can be significantly reduced in the in-control state by adjusting the warning limits. Therefore, this article shows that the risk-based approach can be used effectively in the field of adaptive control charts.

Previous studies (Kosztyán et al., 2017; Kosztyán & Katona, 2016) showed that the risk-based approach can be used in different fields of quality control (conformity control, multivariate control chart). This

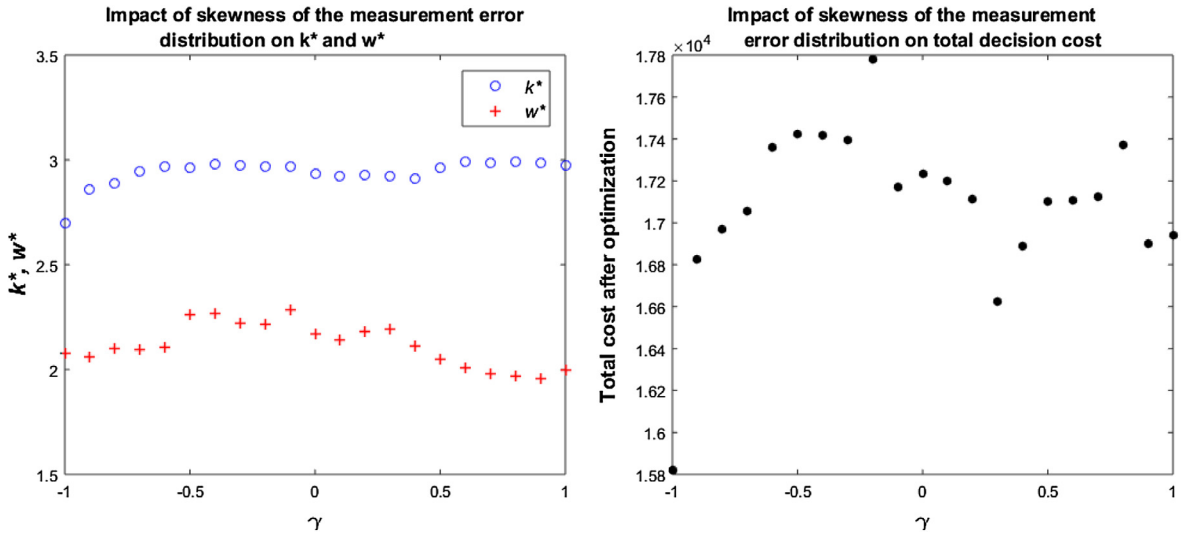

Fig. 9. Sensitivity analysis regarding the skewness of measurement error distribution.

paper confirms that this method can be extended to the field of adaptive control charts but focuses on the VSSI X-bar chart only. Nevertheless, further extension of the approach is required to construct a risk-based family of control charts, including adaptive and multivariate control charts.

Acknowledgements

This research was supported by János Bolyai Fellowship. We acknowledge the financial support of Széchenyi 2020 under the EFOP-3.6.1-16-2016-00015.

Appendix A

To illustrate how the skewness of the measurement error distribution changes, we present a histogram of the measurement error distribution in Fig. 10.

The histogram on the left side of Fig. 10 shows the case when all the measurement error values are considered without creating subgroups. The histogram on the right side was derived from the same lot after creating subgroups with sample size $n = 4$. When calculating the average of each subgroup, the observed measurement error distribution tends to the normal distribution and the skewness changes from -0.8 to -0.4.

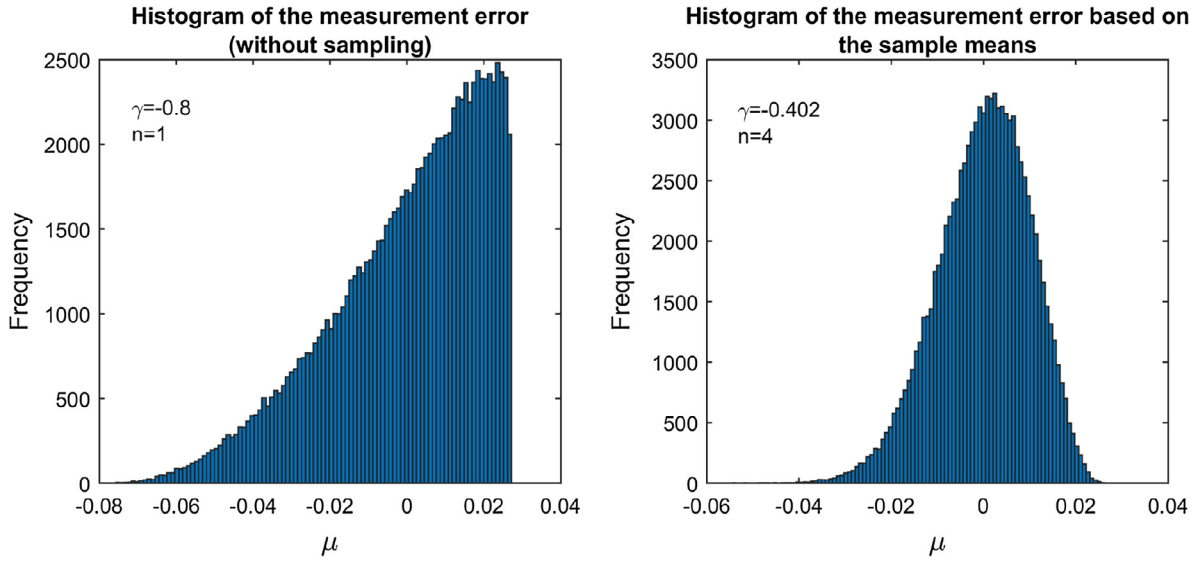

Fig. 10. Histogram of the measurement error before and after the creation of subgroups.

Appendix B

In this Appendix, we also provide the following table including the statements/results we highlighted in this paper. The table was created in order to help the reader to understand which statements are case-specific and which ones can be considered as general (see Table 5).

Table 5
General and Case-specific statements in the paper.

Statement	Case-specific	General
In the case of adaptive control charts, the decision matrix can be extended with the consideration of warning limits		x
The measurement error is not only affecting the decision regarding the control of the process, but also can lead to incorrect sampling policy		x
The proposed method is sensitive for σ_m. However k^* and w^* do not react to the change of skewness (due to central limit theorem)		x
The proposed model is able to reduce the decision cost with 13.5% in the given example	x	
The proposed model can reduce the total decision cost under linearly increasing measurement error variance	x	

References

Abbasi, S. A. (2016). Exponentially weighted moving average chart and two-component measurement error. *Quality and Reliability Engineering International, 32*(2), 499–504.
Aslam, M., Arif, O. H., & Jun, C.-H. (2016). A new variable sample size control chart using mds sampling. *Journal of Statistical Computation and Simulation, 86*(18), 3620–3628.
Bai, D. S., & Lee, K. T. (1998). An economic design of variable sampling interval control charts. *International Journal of Production Economics, 54*(1), 57–64.
Baral, A. K., & Anisa, M. (2015). Assessment of in the presence of measurement errors. *Journal of Statistical Theory and Applications, 14*(1), 13–27.
Chen, Y.-K. (2004). Economic design of variable sampling interval t^2 control charts-a hybrid markov chain approach with genetic algorithms. *Expert Systems with Applications,* (33), 683–689.
Chen, Y.-K., Hsieh, K.-L., & Chang, C.-C. (2007). Economic design of the vssi $\overline{X}$ control charts for correlated data. *International Journal of Production Economics, 107*, 528–539.
Chew, X. Y., Khoo, M. B. C., Teh, S. Y., & Castagliola, P. (2015). The variable sampling interval run sum $\overline{X}$ control chart. *Computers & Industrial Engineering,* (90), 25–38.
Costa, A. F., & Machado, M. A. (2016). A side-sensitive synthetic chart combined with a vss xâĂ chart. *Computers & Industrial Engineering, 91*, 205–214.
Costa, A. F. B. (1994). $\overline{X}$ chart with variable sample size. *Journal of Quality Technology, 26*, 155–163.
Costa, A. F. B. (1997). $\overline{X}$ charts with variable sample size and sampling intervals. *Journal of Quality Technology, 29*(2), 197–204.
Costa, A. F. B. (1998). Joint $\overline{X}$ and r charts with variable parameters. *IIE Transactions, 30*(6), 505–514.
Costa, A. F. B. (1999). Joint $\overline{X}$ and r charts with variable sample sizes and sampling intervals. *Journal of Quality Technology, 31*(4), 387–397.
De Magalhães, M., Costa, A. F. B., & Moura Neto, F. (2009). A hierarchy of adaptive $\overline{X}$

control charts. *International Journal of Production Economics, 119*(2), 271–283.
Fan, S.-K. S., Liang, Y.-C., & Zahara, E. (2006). A genetic algorithm and a particle swarm optimizer hybridized with Nelder-Mead simplex search. *Computers & Industrial Engineering, 50*(4), 401–425 (Sustainability and Globalization: Selected papers from The 32nd. ICC&IE).
Grau, D. (2011). Lower confidence bound for capability indices with asymmetric tolerances and gauge measurement errors. *International Journal of Quality Engineering and Technology, 2*(3), 212–228.
Haq, A., Brown, J., Moltchanova, E., & Al-Omari, A. I. (2015). Effect of measurement error on exponentially weighted moving average control charts under ranked set sampling schemes. *Journal of Statistical Computation and Simulation, 85*(6), 1224–1246.
Hu, X., Castagliola, P., Sun, J., & Khoo, M. B. (2015). The effect of measurement errors on the synthetic x chart. *Quality and Reliability Engineering International, 31*(8), 1769–1778.
Hu, X., Castagliola, P., Sun, J., & Khoo, M. B. (2016a). The performance of variable sample size x chart with measurement errors. *Quality and Reliability Engineering International, 32*(3), 969–983.
Hu, X., Castagliola, P., Sun, J., & Khoo, M. B. C. (2016b). Effect of measurement errors on the vsi x chart. *European Journal of Industrial Engineering, 10*(2), 224–242.
Jensen, W. A., Jones-Farmer, L. A., Champ, C. W., & Woodall, W. H. (2006). Effects of parameter estimation on control chart properties: A literature review. *Journal of Quality Technology, 38*(4), 349.
Kosztyán, Z. T., Hegedűs, C., & Katona, A. (2017). Treating measurement uncertainty in industrial conformity control. *Central European Journal of Operations Research,* 1–22.
Kosztyán, Z. T., & Katona, A. I. (2016). Risk-based multivariate control chart. *Expert Systems with Applications,* (62), 250–262.
Lee, P.-H., Torng, C.-C., & Liao, L.-F. (2012). An economic design of combined double sampling and variable sampling interval $\overline{X}$ control chart. *International Journal of Production Economics,* (138), 102–106.
Lim, S. L., Khoo, M. B. C., Teoh, W. L., & Xie, M. (2015). Optimal designs of the variable sample size and sampling interval $\overline{X}$ chart when process parameters are estimated. *International Journal of Production Economics,* (166), 20–35.
Lin, H.-H., Chou, C.-Y., & Lai, W.-T. (2009). Economic design of variable sampling intervals $\overline{X}$ charts with a&l switching rule using genetic algorithms. *Expert Systems with Applications,* (36), 3048–3055.
Linna, K. W., & Woodall, W. H. (2001). Effect of measurement error on Shewhart control charts. *Journal of Quality Technology, 33*(2), 213–222.
Lira, I. (1999). A bayesian approach to the consumer's and producer's risks in measurement. *Metrologia, 36*, 397–402.
Maleki, M., Amiri, A., & Ghashghaei, R. (2016). Simultaneous monitoring of multivariate process mean and variability in the presence of measurement error with linearly increasing variance under additive covariate model. *International Journal of Engineering-Transactions A: Basics, 29*(4), 471–480.
Maravelakis, P., Panaretos, J., & Psarakis, S. (2004). Ewma chart and measurement error. *Journal of Applied Statistics, 31*(4), 445–455.
Maravelakis, P. E. (2012). Measurement error effect on the cusum control chart. *Journal of Applied Statistics, 39*(2), 323–336.
Mittag, H.-J., & Stemann, D. (1998). Gauge imprecision effect on the performance of the xs control chart. *Journal of Applied Statistics, 25*(3), 307–317.
Naderkhani, F., & Makis, V. (2016). Economic design of multivariate bayesian control chart with two sampling intervals. *International Journal of Production Economics,* (174), 29–42.
Pearn, W., Shu, M., & Hsu, B. (2005). Testing process capability based on cpm in the presence of random measurement errors. *Journal of Applied Statistics, 32*(10), 1003–1024.
Pendrill, L. R. (2008). Operating cost characteristics in sampling by variable. *Accreditation and Quality Assurance,* (13), 619–631.
Prabhu, S. S., Montgomery, D. C., & Runger, G. C. (1994). A combined adaptive sample size and sampling interval $\overline{X}$ control scheme. *Journal of Quality Technology, 27*, 74–83.
Prabhu, S. S., Runger, G. C., & Keats, J. B. (1993). X chart with adaptive sample sizes. *International Journal of Production Research, 31*(12), 2895–2909.
Rahlm, M. (1985). Economic model of x-chart under non-normality and measurement errors. *Computers & Operations Research, 12*(3), 291–299.
Reynolds, M. R., Amin, R. W., Arnold, J. C., & Nachlas, J. A. (1988). $\overline{X}$ charts with variable sampling intervals. *Technometrics, 30*(2), 181–192.
Runger, G., & Pignatiello, J. (1991). Adaptive sampling for process control. *Journal of Quality Technology, 23*(2), 135–155.
Safe, H., Kazemzadeh, R., & Gholipour Kanani, Y. (2018). A Markov chain approach for double-objective economic statistical design of the variable sampling interval control chart. *Communications in Statistics-Theory and Methods, 47*(2), 277–288.
Saghaei, A., Fatemi Ghomi, S., & Jaberi, S. (2014). Economic design of exponentially weighted moving average control chart based on measurement error using genetic algorithm. *Quality and Reliability Engineering International, 30*(8), 1153–1163.
Salmasnia, A., Kaveie, M., & Namdar, M. (2018). An integrated production and maintenance planning model under vp-t2 hotelling chart. *Computers & Industrial Engineering*.
Tagaras, G. (1998). A survey of recent developments in the design of adaptive control charts. *Journal of Quality Technology, 30*, 212–231.
Teoh, W. L., Chong, J., Khoo, M. B., Castagliola, P., & Yeong, W. C. (2017). Optimal designs of the variable sample size x̄ chart based on median run length and expected median run length. *Quality and Reliability Engineering International, 33*(1), 121–134.
Wu, C.-W. (2011). Using a novel approach to assess process performance in the presence of measurement errors. *Journal of Statistical Computation and Simulation, 81*(3), 301–314.
Yang, S.-F. (2002). The effects of imprecise measurement on the economic asymmetric xÌĎ and s control charts. *Asian Journal on Quality, 3*(2), 46–56.
Yeong, W., Khoo, M. B., Tham, L., Teoh, W., & Rahim, M. (2017). Monitoring the coefficient of variation using a variable sampling interval ewma chart. *Journal of Quality Technology, 49*(4), 380–401.
Yue, J., & Liu, L. (2017). Multivariate nonparametric control chart with variable sampling interval. *Applied Mathematical Modelling, 52*, 603–612.
Zhou, M. (2017). Variable sample size and variable sampling interval Shewhart control chart with estimated parameters. *Operational Research, 17*(1), 17–37.